Enhancing water sensing via aggregation-induced emission (AIE) and solvatofluorochromic studies using two new dansyl derivatives containing a disulfide bound: Pollutant metal ions detection and preparation of water-soluble fluorescent polymeric particles

Frederico Duarte [a], Georgi Dobrikov [b*], Atanas Kurutos [b, c], Hugo M. Santos [a,d],
Javier Fernández-Lodeiro [a,d], Jose Luis Capelo-Martinez [a,d], Elisabete Oliveira [a,d*], Carlos Lodeiro [a,d*]

[a] BIOSCOPE Research Group, LAQV-REQUIMTE, Chemistry Department, NOVA School of Science and Technology, FCT NOVA, Universidade NOVA de Lisboa, 2829-516 Caparica, Portugal
[b] Institute of Organic Chemistry with Centre of Phytochemistry, Bulgarian Academy of Sciences,
Acad. G. Bonchev str., bl. 9, 1113 Sofia, Bulgaria
[c] University of Chemical Technology and Metallurgy, 8 St. Kliment Ohridski blvd, 1756 Sofia, Bulgaria
[d] PROTEOMASS Scientific Society,
Rua dos Inventores, Madam Parque, Caparica Campus, 2829-516 Caparica, Portugal

* Corresponding authors: Georgi.Dobrikov@orgchm.bas.bg (GD); ej.oliveira@fct.unl.pt (EO) and cle@fct.unl.pt (CL)

Abstract

Polarity-sensitive dansyl derivatives **L1** and **L2** were synthesized and their ability to sense pollutant metal ions was investigated. All compounds were found to be highly sensitive towards Cu^{2+} and Hg^{2+} metal ions, while **L2** being able to detect and quantify Hg^{2+} concentrations as low as 2.5 μM. Both **L1** and **L2** exhibit positive solvatofluorochromic behaviour, modulated in the presence of water, which in turn results in fluorescence enhancement *via* aggregation-induced emission (AIE). Seeking stability and water solubility, luminescent **L1**-based polystyrene-block-polybutadiene-block-polystyrene (SBS) microparticles (size: 520 ± 76 nm) were successfully prepared while maintaining the fluorescence emission of fluorophore **L1** (ϕ = 22%). This work stands up the dansyl-derivatives multiple properties and their promising applications in biomedicine and environmental fields.

Keywords: polystyrene-block-polybutadiene-block-polystyrene (SBS) microparticles, dansyl derivatives, metal ions, AIE effect, solvatochromism

1. Introduction

Over the past decades, the unique properties of dansyl derivatives have made them a useful tool for environmental science, analytical chemistry, biosensors and biological imaging [1-9]. The low intensity-excitation wavelengths of dansyl derivatives and high fluorescence quantum yield, provide strong conditions to be applied as biological probes and in the development of chemical sensors for the detection of heavy and transition metal ions [10]. The high sensitivity and selectivity of the dansyl moiety enhance the applicability for detecting these ions at low concentrations in the environment. The rather low detection limits reported of the dansyl derivatives for Cu^{2+}, ranging between 0.2 µM and 0.9 µM for Cu^{2+} and 140 nM for Hg^{2+}, respectively, turn it a valuable vehicle for pollution control and environmental monitoring [11], [12], [13]. Additionally, their solvatochromic effect makes them suitable for imaging and environmental control, since changes in solvent polarity result in wavelength shifts in the absorption and emission bands [1].

Numerous organic dyes express excellent fluorescent properties in solution, however, at higher concentrations or in the solid state, aggregation of these dyes results in a decrease in the intensity emission signal, due to non-radiative transitions. Since the first discovery in 2001 of fluorophores with aggregation-induced emission (AIE) reported by *Tang et. al.* [14], increasing popularity has been observed due to their high sensitivity, and selectivity [15–18]. In the AIE water-based mechanism, water modulates the aggregation state of the fluorophore, resulting in fluorescence enhancement, providing a simple and direct way to monitor water content in complex environments, such as biological samples and industrial processes [19–21].

Despite the plethora of available analytical methods for water detection, fluorescence-based techniques stands out to be the most rapid, sensitive and cost-effective approach. In fluorescent-based water sensors, as organic molecules, water can be detected by employing fluorescence "turn-off", "turn-on" or ratiometric methods. In the previous methods, photo-induced electron transfer (PET) and aggregation-induced emission (AIE) are some of the mechanisms discussed [21]. Among others, dansyl derivatives have been widely used as water sensors in organic solvents since they exhibit a strong fluorescence response to water content [21]. AIE platform has also been extensively used as a metal ion- responsive luminescent probe due to its sensitivity to the environment [22], [23].

However, the hydrophobicity of AIE-active organic compounds is still a challenging task when considering aqueous media applications. This challenge could be hampered by developing water soluble polymeric nanoparticles, opening up new opportunities in biomedicine and environmental areas [24], [25].Fluorescent dye-doped polymer nanoparticles have shown great potential, providing significant improvements in sensitivity, stability, and enhanced fluorescence being many fold-brighter compared to traditional organic dyes. Dye-loaded polymer NPs allow high dye loading without aggregation-caused quenching (ACQ). Only recently were reported strategies to overcome ACQ in polymer nanoparticles, such as the design of organic compounds with the ability of AIE, resulting in increased fluorescence quantum yield and photostability [2], [26–29].

For more than twenty years the main focus of our research group has been devoted to sensing pollutant metal ions and anions using fluorescent polyamines [30-32], macrocycles, porphyrins or corroles [33], [34], sulphur-containing sensors [35], and nanoparticles [36].

Based on our experience, in this work two dansyl derivatives (**L1** and **L2**) were synthesized and fully characterized. Aiming the creation of new breakthroughs in the state of the art, the multiple properties and advantages abovementioned of dansyl derivatives were fully explored, such as (i) the solvatochromic effect, (ii) sensing ability towards pollutant metal ions, (iii) water detection in organic solvent *via* AIE, photostability, as well as (iv) the production of dansyl derivative (**L1**) doped polystyrene-block-polybutadiene-block-polystyrene (SBS) microparticles (L1@SBS) [37], aiming higher fluorescence quantum yields *via* AIE in water.

2. Experimental Section

2.1. Materials

The metal salts: $Cu(OTf)_2$, $Cd(OTf)_2$, $Co(OTf)_2$, $Ag(OTf)$, $Pb(OTf)_2$, $Zn(OTf)_2$, $Ni(OTf)_2$ and $Ca(OTf)_2$ were purchased from Solchemar, and $Hg(OTf)_2$, dansyl amide and all solvents have been acquired from Sigma Aldrich without requiring additional steps of purification. Spectroscopy grade solvents were used for measurement of electronic spectra and fluorescence – acetonitrile (CH_3CN), chloroform ($CHCl_3$), toluene, ethanol (EtOH), dimethylsulfoxyde (DMSO) and tetrahydrofurane (THF). Poly(styrene-butadiene-styrene) (SBS) was purchased from Sigma-Aldrich (St. Louis, MO, USA). Mili-Q ultrapure water was used in all experiments. The analytical grade reagents and solvents needed for the synthesis of the target dansyl derivatives were purchased from Alfa Aesar, Fluka, Fluorochem Ltd, Merck, TCI, and Sigma-Aldrich, and were utilized as received. TLC was used to monitor the reaction outcome (Merck silica gel 60 F254 precoated TLC plates - 0.2 mm thick). Purification of the crude products was achieved by column chromatography employing silica gel as a stationary phase. Details about the employed mobile phases are given in the corresponding synthetic protocols listed bellow.

2.2. Instrumentation

Dynamic light scattering (DLS) data has been obtained from a Malvern Zetasizer Nano series (Worcestershire, WR14 1XZ, UK) from PROTEOMASS Scientific Society-BIOSCOPE Facility Lab. Samples have been analyzed at a scattering angle of 90° and at a temperature of 25°C while supported in a glass cell. The z-potential measurement of micro and nanoparticles were performed using a dip-cell. High-Resolution Mass Spectrometry analyses were carried out in the Laboratory for Biological Mass Spectrometry–Isabel Moura (PROTEOMASS Scientific Society Facility), using UHR ESI-Qq-TOF IMPACT HD (Bruker-Daltonics, Bremen, Germany). Compounds were dissolved in 50% (v/v) Acetonitrile containing 0.1% (v/v) aqueous formic acid to obtain a working solution of 0.1 µg/mL. Mass spectrometry analysis was carried out by the direct infusion of the compound solutions into the ESI source. MS data were acquired in positive polarity over the mass range of 80 – 1300 m/z. (Capillary voltage: 4500 V, End

plate offset: -500 V, Charging voltage: 2000 V, Corona: 4000 nA, Nebulizer gas: 0.4 Bar, Dry Heater: 180°C, Dry gas: 4.0 L/min).

Transmission electron microscopy (TEM) images were obtained using a JOEL JEM 1010 transmission electron microscope from the CACTI, University of Vigo (Spain), operating at 100 kV. Samples have been prepared by dropping 5 µL of the colloidal suspension on a copper grid coated with a continuous carbon film, and the solvent was allowed to evaporate. The size of particles and histograms were calculated from TEM images using the ImageJ software (Image 1.51h, Wayne Rasband, National Institutes of Health, Bethesda, MD, USA).

UV-Vis absorption spectra were recorded with a JASCO V-650 spectrophotometer and a fluorescence emission by a HORIBA Scientific FLUOROMAX-4 spectrofluorimeter from PROTEOMASS Scientific Society Facility. All samples were carried out at 293 K with recourse to rectangular quartz cells of 10 mm in width. Visualization of the TLC was performed using a Vilber UV Lamp (BVL-6.LC dual wavelength 254 nm/365 nm, operational power of 2×6 Watts). Using a combination of ^{1}H-NMR, ^{13}C-NMR, and high-resolution mass spectrometry, all compounds' chemical identities were verified. Using 5 mm tubes on a Bruker Avance II+ 600 spectrometer, the ^{1}H-NMR and ^{13}C-NMR spectra were measured in $CDCl_3$ at 293 K at operating frequencies of 600.13 MHz and 150.92 MHz, respectively. Chemical shifts are measured to an accuracy of 0.01 parts per million (ppm). The coupling constants (J) are shown with a precision of 0.1 and represented in Hz. The spin multiplicity in the 1H-NMR was denoted by the abbreviations s = singlet, d = doublet, t = triplet, q = quartet, dd = doublet of doublets, dt = doublet of triplets, td = triplet of doublets, and m = multiplet.

2.3.   Synthetic procedures

2.3.1. Synthesis of **L1** and **L2**

Synthesis of intermediate N,N'-(disulfanediylbis(ethane-2,1-diyl))bis(2-aminobenzamide) (3):

In a 100 ml flask charged with 50 mL dry dichloromethane (DCM) were added consequently anthranilic acid (**2**) (0.600 g, 4.38 mmol, 2.2 eq.), diamine **1** as di-HCl salt (0.450 g, 1.99 mmol, 1.0 eq.), diisopropylethylamine (DIPEA) (1.54 g, 1.97 mL, 11.93 mmol, 6.0 eq.) and TBTU (1.41 g, 4.38 mmol, 2.2 eq.). The formed clear solution was stirred at r.t. for 41 h. TLC of reaction mixture – DCM:methyl-*tert*-butyl ether (MTBE) = 5:1, x2. Workup: dilution with 30 mL DCM and washing with 1% aq. citric acid, sat. aq. $NaHCO_3$ and finally with water. The organic phase was dried over anhydrous Na_2SO_4, filtered and evaporated to dryness. This crude product was purified by column chromatography: 75 g silica; phase 1 - DCM:MTBE=5:1 (to remove contaminations); phase 2 - DCM:MTBE=5:2 (for product). After solvent evaporation and drying *in vacuo,* product **3** was obtained as a white powder (0.760 g, 99%). m.p. 132-133°C. ^{1}H NMR (600 MHz, $CDCl_3$) δ 7.38 (dd, J = 7.9, 1.5 Hz, 1H), 7.20 (ddd, J = 8.3, 7.2, 1.5 Hz, 1H), 6.78 (s, 1H), 6.72 – 6.57 (m, 2H), 5.48 (s, 2H), 3.76 (q, J = 6.3 Hz, 2H), 2.95 (t, J = 6.4 Hz, 2H), 2.17 (s, 4H). ^{13}C NMR (151 MHz, $CDCl_3$) δ 207.24, 169.70, 148.87, 132.59, 127.52, 117.44, 116.79, 115.82, 38.72, 38.15, 31.10 (Figures S1, S2).

*Synthesis of N,N'-(disulfanediylbis(ethane-2,1-diyl))bis(2-((5-(dimethylamino)naphthalene)-1-sulfonamido)benzamide) (**L1**)*

Compound **3** (0.300 g, 0.77 mmol, 1.0 eq.) was dissolved in 5 mL dry pyridine. Then dansyl chloride (0.456 g, 1.69 mmol, 2.2 eq.) was added and formed clear solution was stirred at r.t. for 72 h. Workup: excess of conc. aq. citric acid was added and extracted with DCM. The organic phase was washed with water, dried over anhydrous Na_2SO_4, filtered and evaporated to dryness. This crude product was purified by column chromatography: 70 g silica, phase DCM:MTBE=20:1. After solvent evaporation and drying *in vacuo*, product **L1** was obtained as a yellow powder (0.510 g, 78%). m.p. 123-124°C. ^1H NMR (600 MHz, $CDCl_3$) δ 11.17 (s, 2H), 8.46 (dt, J = 8.6, 1.1 Hz, 2H), 8.32 (d, J = 8.7 Hz, 2H), 8.23 (dd, J = 7.3, 1.2 Hz, 2H), 7.55 – 7.47 (m, 4H), 7.43 (dd, J = 8.5, 7.3 Hz, 2H), 7.30 (dd, J = 7.9, 1.5 Hz, 2H), 7.29 – 7.23 (m, 2H), 7.12 (d, J = 7.5 Hz, 2H), 6.88 (td, J = 7.6, 1.1 Hz, 2H), 6.62 (t, J = 5.9 Hz, 2H), 3.54 (q, J = 6.3 Hz, 4H), 2.82 (s, 12H), 2.78 (t, J = 6.4 Hz, 4H). ^{13}C NMR (151 MHz, $CDCl_3$) δ 168.80, 151.91, 138.85, 134.77, 132.76, 130.91, 130.05, 129.93, 129.60, 128.52, 127.02, 123.15, 123.13, 120.67, 119.98, 119.09, 115.44, 45.53, 38.96, 37.55. ESI-HRMS: $[M+H]^+$ for $C_{42}H_{44}N_6O_6S_4$ = 857.2270 (- 0.9 ppm), $[M+2H]^{2+}$ $C_{42}H_{44}N_6O_6S_4$ = 429.1175 (- 0.1 ppm). Calculated $[M+H]^+$ for $C_{42}H_{44}N_6O_6S_4$ = 857.227794, and $[M+2H]^{2+}$ $C_{42}H_{44}N_6O_6S_4$ = 429.117535 (Figures S3, S4, S7).

*Synthesis of N,N'-(disulfanediylbis(ethane-2,1-diyl))bis(5-(dimethylamino)naphthalene-1-sulfonamide) (**L2**)*

Diamine **1** as di-HCl salt (0.250 g, 1.11 mmol, 1.0 eq.) and Et_3N (0.560 g, 0.77 mL, 5.55 mmol, 5.0 eq.) were dissolved in 50 mL dry DCM and cooled to 5°C (with ice-water). Then dansyl chloride (0.659 g, 2.44 mmol, 2.2 eq.) was added at once and the formed clear mixture was stirred for 30 min at 5°C, followed by 20 h at r.t. TLC of reaction mixture – DCM:MTBE=5:1, x1. Workup: dilution with 30 mL DCM and washing with 1% aq. citric acid and water. The organic phase was dried over anhydr. Na_2SO_4, filtered and evaporated to dryness. This crude product was purified by column chromatography: 70 g silica, phase DCM:MTBE=10:1. After evaporation of phase and drying *in vacuo*, product **L2** was obtained as a yellow powder (0.65 g, 95%). m.p. 74-75°C. ^1H NMR (600 MHz, $CDCl_3$) δ 8.54 (dd, J = 8.5, 1.1 Hz, 2H), 8.27 – 8.22 (m, 4H), 7.55 (dd, J = 8.7, 7.5 Hz, 2H), 7.52 (dd, J = 8.5, 7.3 Hz, 2H), 7.18 (dd, J = 7.6, 0.9 Hz, 2H), 5.21 (t, J = 6.3 Hz, 2H), 3.10 (q, J = 6.3 Hz, 4H), 2.89 (s, 12H), 2.49 (t, J = 6.3 Hz, 4H). ^{13}C NMR (151 MHz, $CDCl_3$) δ 152.19, 134.51, 130.83, 130.00, 129.82, 129.60, 128.74, 123.32, 118.68, 115.43, 45.55, 41.70, 37.86. ESI-HRMS: $[M+H]^+$ for $C_{28}H_{34}N_4O_4S_4$ = 619.1543 (1.2 ppm), and $[M+2H]^{2+}$ for $C_{28}H_{34}N_4O_4S_4$ = 310.0811 (2.2 ppm). Calculated $[M+H]^+$ for $C_{28}H_{34}N_4O_4S_4$ = 619.153566 and $[M+2H]^{2+}$ for $C_{28}H_{34}N_4O_4S_4$ = 310.080421 (Figures S5, S6, S8).

2.4. Spectrophotometric and spectrofluorimetric measurements

2.4.1. Photophysical characterization and titrations

The spectroscopic characterizations and titrations were performed using stock solutions of compounds **L1** and **L2** (ca. 10^{-3} M) in various organic solvents (CH_3CN, EtOH, DMSO, $CHCl_3$, toluene and THF),

prepared by dissolving the appropriate amount of the selected compound in a 10 mL volumetric flask. The studied solutions were prepared by appropriate dilution of the stock solutions up to $10^{-5} – 10^{-6}$ M. Titrations of **L1** and **L2** were carried out by the addition of microliter amounts of standard solutions of Ca^{2+}, Co^{2+}, Ni^{2+}, Cu^{2+}, Zn^{2+}, Ag^+, Cd^{2+}, Hg^{2+}, Pb^{2+} ions in acetonitrile. A correction for the absorbed light was performed when necessary.

Spectra of solid samples were collected with a Horiba-Jobin-Yvon Fluoromax-4® spectrofluorometer using an optic fibre connected to the equipment, by exciting the solid compounds at appropriated λ (nm). All measurements were performed at 298 K.

Additionally, mixtures containing different water fractions (f_w), (f_w = 0%, 17%, 33%, 55%, 67% and 83%) with a final concentration of 10 mM were prepared and characterized by absorption and emission spectroscopy.

Table 1. Spectroscopic polarity parameters, physical properties of the different solvents. ε_r : relative permittivity; η: refractive index; α: the solvent's HBD acidity; β: the solvent's HBA basicity; π^*: the solvent's dipolarity/polarizability.

Solvent	ε_r	α	β	π^*	η
DMSO	47.24	0	0.76	1.00	1.47
CH₃CN	35.94	0.19	0.40	0.66	1.34
EtOH	24.30	0.86	0.75	0.54	1.36
THF	7.58	0	0.55	0.58	1.40
CHCl₃	4.89	0.20	0.10	0.69	1.44
Toluene	2.38	0	0.11	0.54	1.49

2.4.2. Fluorescence quantum yield and Lifetime

Relative photoluminescence quantum yields were performed using as the standard a solution of dansyl amide in acetonitrile for quantifying the relative QY of both compounds dissolved in the same solvent (ϕ_F = 0.37), while the remaining ones have been measured relative to the standard solution of dansyl amide in DMSO (ϕ_F = 0.61), as well as for both compounds in f_w = 83% [38]. The quantum yield for the polymeric particles of **L1** was obtained relative to the compound itself in chloroform. Tempro Fluorescence Lifetime System with a Nanoled pulsed diode controller from Horiba Jobin-Yvon (PROTEOMASS Scientific Society Facility) was used to perform lifetime measurements.

2.5. Synthesis of L1 polymeric microparticles

A solution of polymer matrix styrene-butadiene-styrene block copolymer (SBS) (50 mg) in 2 mL of tetrahydrofuran (THF) was prepared and heated at 70°C for 5 min aiming to allow solubilization. When the solution was cooled back to room temperature, an aliquot of 0.6 mL was quickly added to **L1** (0.5 mg) and transferred over 2.4 mL of deionized water, maintaining a magnetic stirring at 400 rpm for 5 min. The resulting mixture was stored at 20°C in the dark for 24 h for oil-in-water droplets stabilization. The final particles were obtained after evaporation of THF at room temperature for 24 h. Before use, a filtration step using glass membranes with a pore size of 10–15 µm was performed to remove potential non-encapsulated **L1** and polymer precipitates.

2.6. Determination of the detection and quantification limits (LOD and LOQ)

For the determination of the detection limit (LOD) and quantification limit (LOQ), ten different measurements of a solution containing the selected probe were collected without the addition of any metal ion (y_{blank}). The LOD and LOQ were determined by the formulas:

LOD = y_{dl} = y_{blank} + 3std, where y_{dl} = signal detection limit and std = standard deviation.

LOQ = y_{dl} = y_{blank} + 10std, where y_{dl} = signal detection limit and std = standard deviation.

Additionally, small amounts of the metal ion were added to a solution containing **L1** and **L2**, to determine the minimal detectable and quantified concentration out of the LOD and LOQ values, respectively.

3. Results and Discussion

3.1. Synthesis

The synthesis of the target sulfonamides **L1** and **L2** was accomplished according to Scheme 1. Compound **L1** was synthesized in two steps. The first step includes the preparation of intermediate **3** quantitative starting from anthranilic acid (**2**) and **1** (both commercial products) proceeding atambient temperature, by implementation of classical conditions of the peptide synthesis - presence of coupling reagent 2-(1*H*-benzotriazole-1-yl)-1,1,3,3-tetramethylaminium tetrafluoroborate (TBTU) under basic conditions (excess of DIPEA in dichloromethane). After isolation and purification, compound **3** was reacted with commercial dansyl chloride in dry pyridine (Py) at r.t. to furnish **L1** in 78% yield. Direct acylation of the diamine **1** with dansyl chloride (with excess of tryethylamine) in dry dichloromethane (DCM) affords the target product **L2** in 95% yield. The preparation of this compound was previously reported in the literature, concerning an investigation of fluorescent thiomaleimides [39].
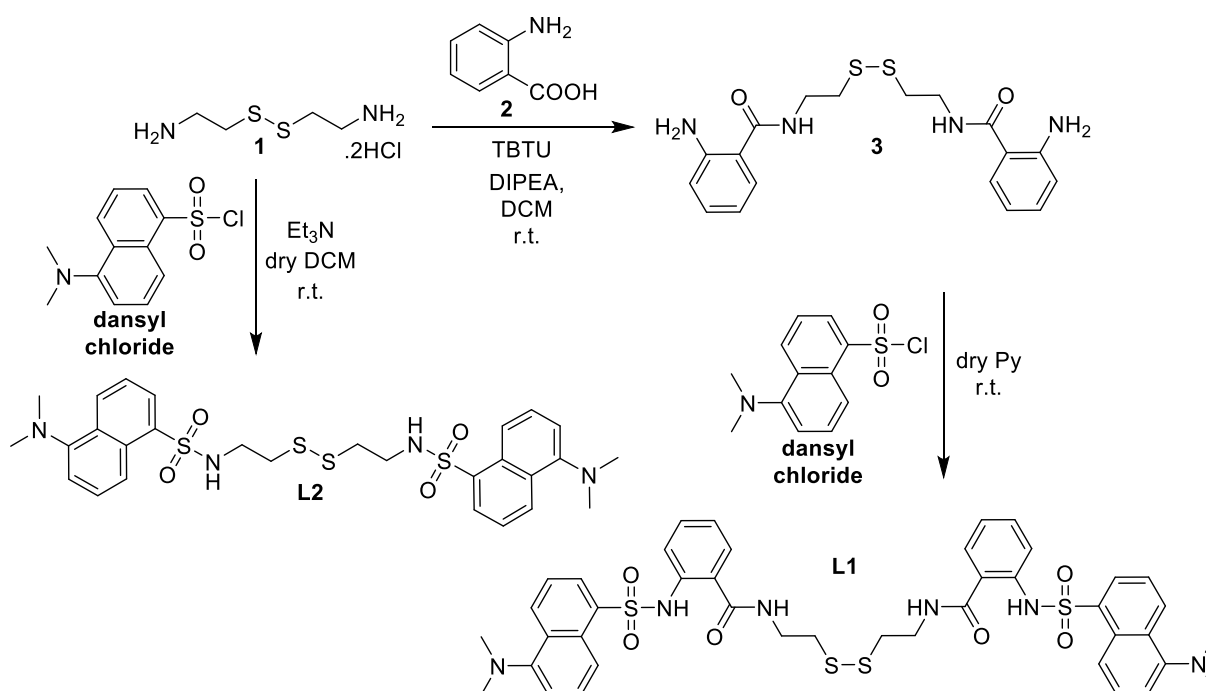
Scheme 1. Synthetic approach to the preparation of the target **L1** and **L2** fluorophores.

3.2. Photophysical characterization

Figure 1 shows the main photophysical characterization of **L1** and **L2** evaluated at 298 K in acetonitrile. Compounds **L1** and **L2** exhibit two main absorption bands at 332 nm and 340 nm, respectively, which is a hallmark of the π-π* transition of the dansyl chromophore, being naked-eye colourless. Concerning the emission properties, fluorophore **L1** shows a maximum emission band located at 527 nm and **L2** at 518 nm, both of which emitting an intense green colour under UV light. In the solid state, the emission of both compounds is characterized by a pronounced blue-shift of about 20 nm compared to the solution. Hence, 507 nm and 499 nm for **L1** and **L2**, respectively. The incorporation of a benzene ring as in the case of **L1** leads to a red-shift in the emission wavelength, as well as, in solid state compared to **L2**, due to extending the conjugation, with the consequent decrease in fluorescence quantum yield and brightness, rendering a compound less stable in the excited state, thus shortening its lifetime (see Figure 1D).
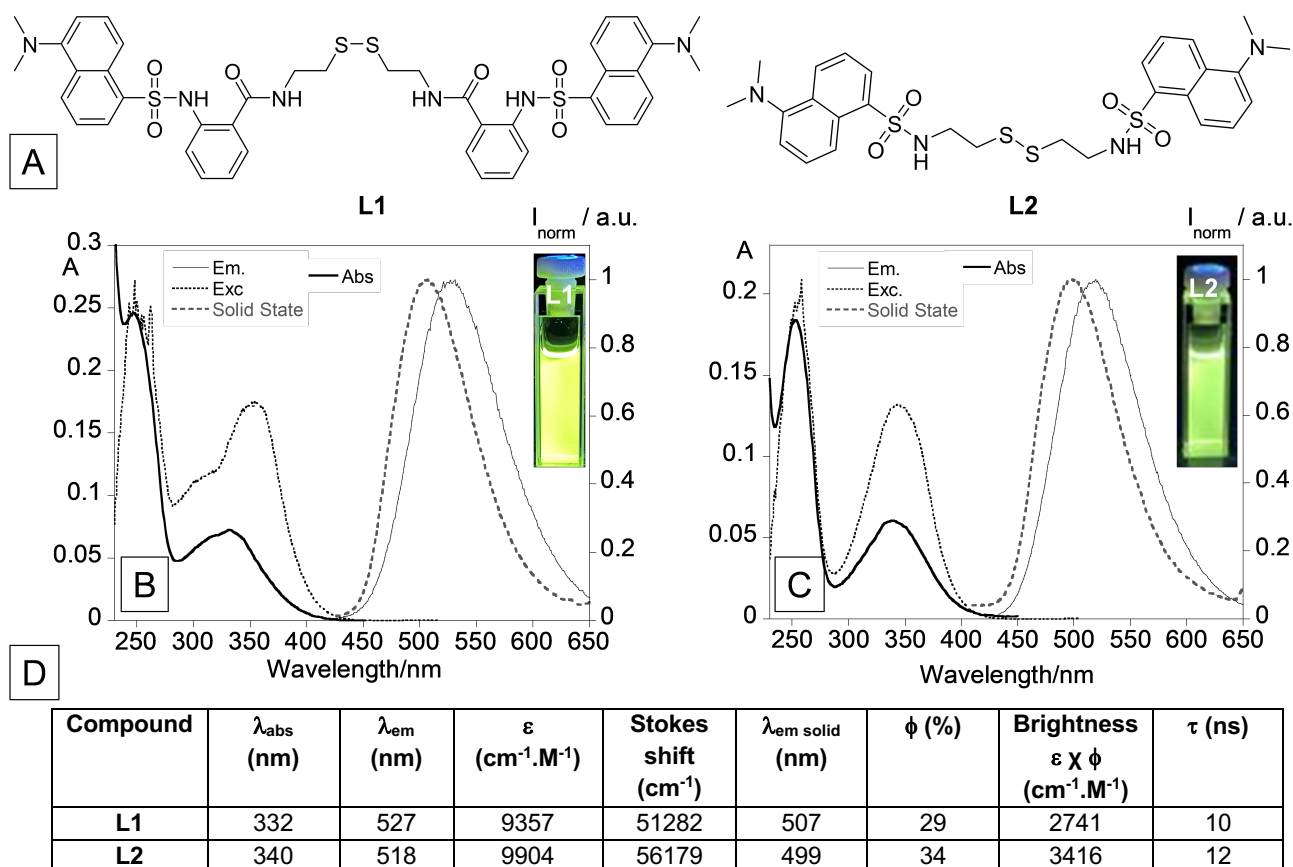

Compound	λ_{abs} (nm)	λ_{em} (nm)	ε (cm^{-1}.M^{-1})	Stokes shift (cm^{-1})	$\lambda_{em\ solid}$ (nm)	ϕ (%)	Brightness $\varepsilon \times \phi$ (cm^{-1}.M^{-1})	τ (ns)
L1	332	527	9357	51282	507	29	2741	10
L2	340	518	9904	56179	499	34	3416	12

Figure 1. (A) Chemical structure of dansyl derivatives **L1** and **L2**. Absorption, excitation, emission and solid-state emission spectra for **L1** (B) and **L2** (C) in CH$_3$CN ([**L1**]=[**L2**]= 6 µM). (D) Main photophysical data of compounds **L1** and **L2**.

In order to evaluate the sensitivity of **L1** and **L2** to solvent polarity, both compounds were characterized and studied in six different solvents, including DMSO, CH$_3$CN, EtOH, THF, CHCl$_3$ and toluene (Figures S9-S12).

As can be seen in Table 2, in absorption despite their different maximum bands in all solvents, there is no correlation with the solvent polarity increase. However, in the emission, a red shift of the maximum bands is verified, from 498 nm to 535 nm in **L1** and from 488 nm to 520 nm in **L2**, as the polarity of the solvent increase.

Table 2. Photophysical data of the dansyl derivatives **L1** and **L2** evaluated in organic solvents.

Solvent	λ (nm)				ε $(10^4\ cm^{-1}.M^{-1})$		Stokes shift (cm^{-1})		ϕ (%)		τ (ns)	
	L1 (Abs.)	L1 (Em.)	L2 (Abs.)	L2 (Em.)	L1	L2	L1	L2	L1	L2	L1	L2
DMSO	347	535	337	520	1.0506	1.3706	53191	54644	30	59	14	17
EtOH	330	520	338	514	0.9058	1.1285	52631	56818	24	33	13	13
THF	336	507	336	497	1.1135	1.2022	58479	64102	47	50	13	12
CHCl$_3$	343	504	340	498	0.8526	1.0200	62111	62500	52	56	14	15
Toluene	341	498	338	488	1.0325	0.8259	63694	66666	49	57	12	12

Thus, in the excited state polar solvents appear to have a significant impact on the stabilization of the compounds, being **L1** and **L2** more stable in the excited state than in the ground state. Based on the shifts observed in the emission spectra, **L1** and **L2** are denominated positive solvatofluorochromic. This phenomenon has important applications in imaging, biology and biomedicine to measure local polarity in biological structures [40].

To shed more light on the **L1** and **L2** solvatofluorochromic behaviour, and to quantitatively characterize the solute-solvent interactions, the multiparametric fitting of the Kamlet-Taft equation (Equation 1) was performed allowing the determination of the three solute-dependent parameters (υ_0, a, b and p).

$$\upsilon = \upsilon_0 + a\alpha + b\beta + p\pi^* \quad \text{(Equation 1)}$$

where υ_0 is the value of emission in a reference solvent; parameters a, b and p are the responses of the solute property to the solvent property, α: hydrogen bonding acceptor ability polarity scale; β: hydrogen bonding donor ability polarity scale; π^*: dipolarity/polarizability polarity scale (Table 1) [41], [42].

Figure 2 shows the images of **L1** and **L2** under a UV light lamp and based on the fitting linear plots of $\upsilon_{exp.}$ versus $\upsilon_{calc.}$, the fitted parameters ($\upsilon0$, a, b and p), the slope and correlation coefficients.

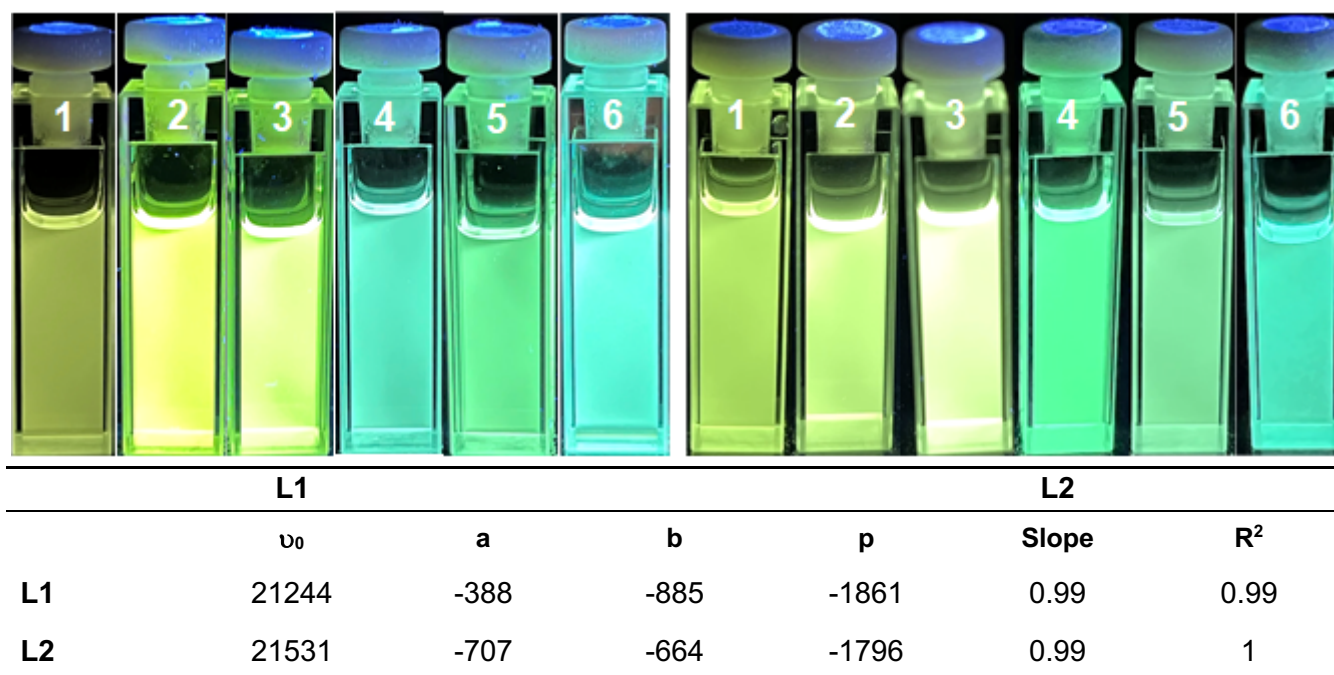|	L1				L2	
	υ_0	a	b	p	Slope	R^2
L1	21244	-388	-885	-1861	0.99	0.99
L2	21531	-707	-664	-1796	0.99	1

Figure 2. (Top) Images of **L1** and **L2** under a UV light lamp. Polarity decrease from 1 to 6 (1 – DMSO; 2 – CH$_3$CN; 3 – EtOH; 4 – THF; 5 – CHCl$_3$; 6 – toluene). (Down) υ_0, a, b and p-values, in cm^{-1}, slope and correlation coefficients obtained from Kamlet–Taft multiparametric fitting of the emission data.

According to the Kamlet-Taft parameters of each compound, **L2** is more polar than **L1**, which could be attributed to differences in their molecular structure. On the other hand, **L1** has the highest polarizability, having the ability to be distorted by an external electric field, which could also be related to its molecular size and shape.

3.3. Metal Ions Sensing

The sensorial ability of dansyl derivatives **L1** and **L2** was studied towards metal ions, such as, Ca^{2+}, Co^{2+}, Ni^{2+}, Cu^{2+}, Zn^{2+}, Ag$^+$, Cd^{2+}, Hg^{2+} and Pb^{2+} in acetonitrile. Figure 3 shows the maximum emission at 527 nm and 518 nm of **L1** and **L2** upon the addition of 1, 5 and 10 equivalents of the above-mentioned metal ions. Both compounds showed unprecedented sensitivity to Cu^{2+} and Hg^{2+} metal ions (see Figure 3).
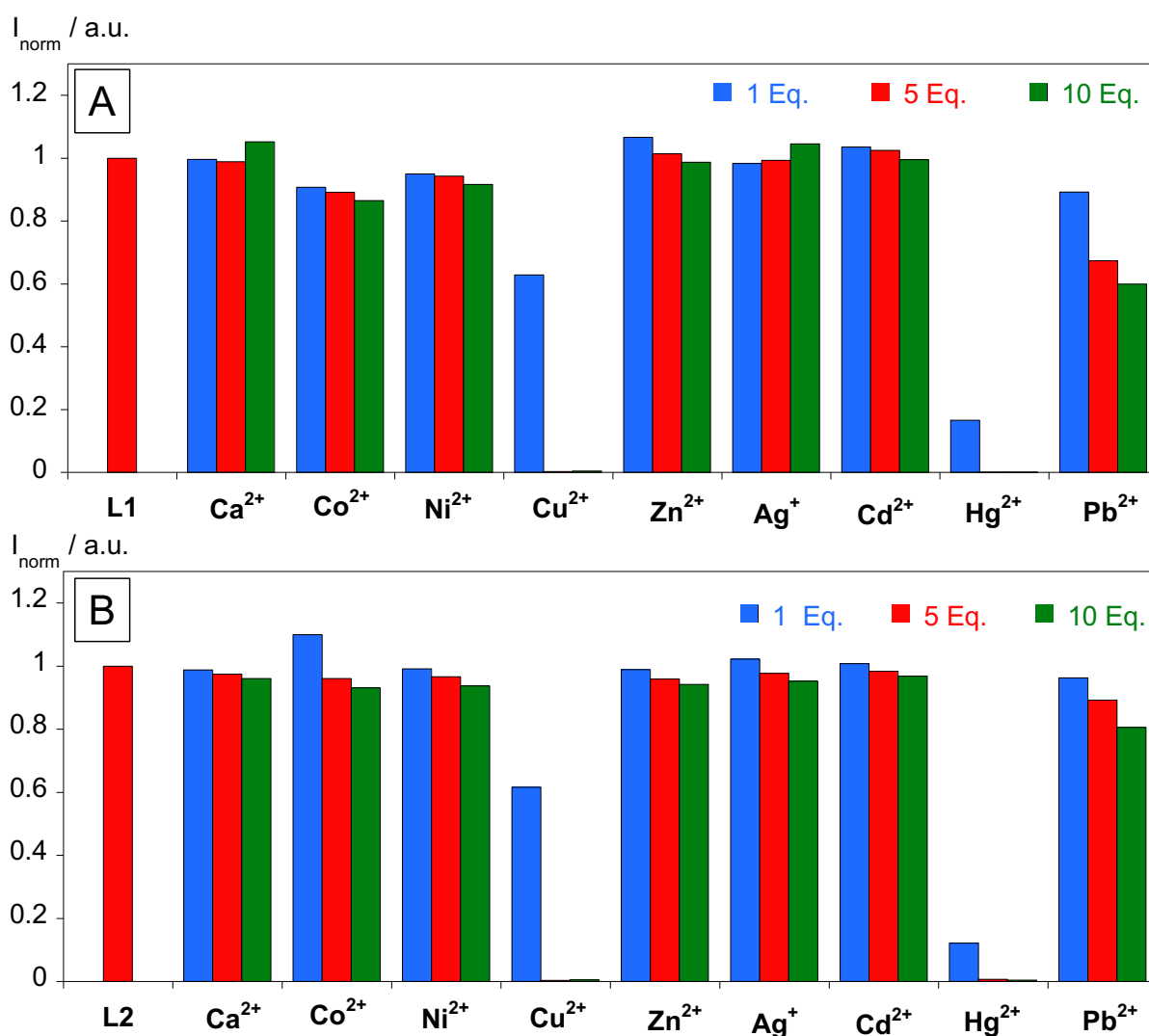
Figure 3. Maximum emission intensities of **L1** (A) and **L2** (B) upon the addition of 1, 5 and 10 equivalents of Ca^{2+}, Co^{2+}, Ni^{2+}, Cu^{2+}, Zn^{2+}, Ag^+, Cd^{2+}, Hg^{2+} and Pb^{2+} metal ions. ([**L1**] =[**L2**] = 20µM, λ_{emL1} = 527 nm, λ_{emL2} = 518 nm, T = 298K).

Figure 4 represents the absorption and emission spectra at increasing amounts of Cu^{2+} (A, C) and Hg^{2+} (B, D) for **L1** and **L2**, respectively. The addition of Cu^{2+} and Hg^{2+} promotes similar spectral behaviour in the absorption, where it is observed a decrease in the absorption at 332 nm, 340 nm and an increase in the absorbance at 290 nm and 255 nm for **L1** and **L2**, respectively. Regarding the emission spectra, in both cases, a quenching in the emission intensity at 527 nm (**L1**) and 518 nm (**L2**) is visualized.
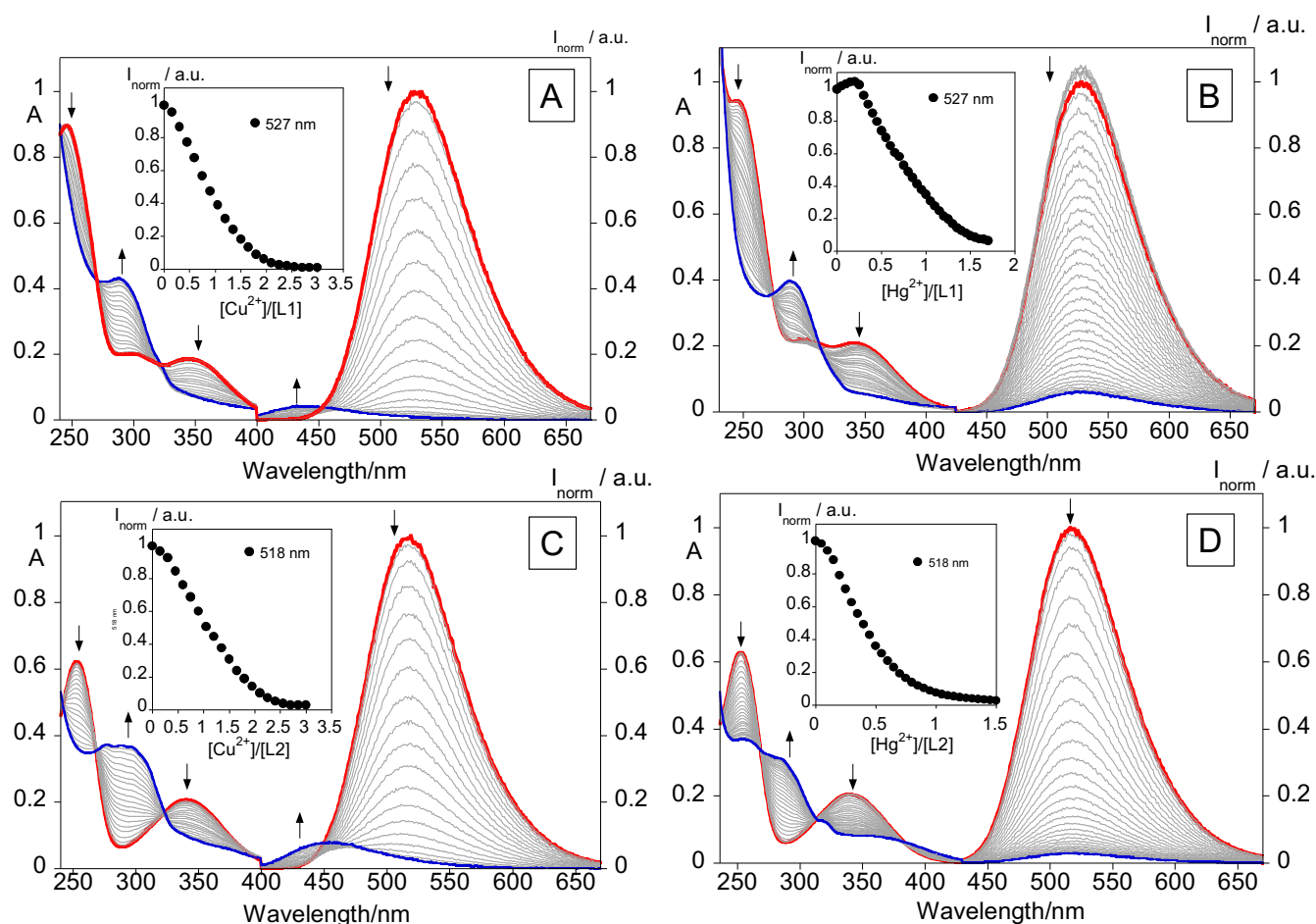
Figure 4. Spectrophotometric and spectrofluorimetric titrations of compounds **L1** (A, B) and **L2** (C, D) with increased additions of Cu^{2+} (A, C), and Hg^{2+} (B, D) in CH_3CN. The inset represents the emission (A-D) as a function of $[Cu^{2+}]/[$**L1**$]$ at 527 nm (A), of $[Cu^{2+}]/[$**L2**$]$ at 518 nm (C), of $[Hg^{2+}]/[$**L1**$]$ at 527 nm (B) and of $[Hg^{2+}]/[$**L2**$]$ at 518 nm (D). $[$**L1**$] = [$**L2**$] = 20$ μM, $\lambda_{excL1}=332$ nm, $\lambda_{excL2}=340$ nm, T = 298 K).

The stability constants were calculated through HypSpec program [43], as well as the minimal detectable and quantified amount of Cu^{2+} and Hg^{2+} in acetonitrile for both compounds and the data are summarized in Table 3.

Table 3. Stability association constants and stoichiometry for the complexes formed **L1** and **L2** with Cu^{2+} and Hg^{2+} ions, in CH_3CN. Minimal detectable (LOD) and quantified (LOQ) amounts (μM) of Cu^{2+} and Hg^{2+} metal ions (M) **L1** and **L2**. LOD and LOQ were measured by emission at 527 nm and 518 nm for **L1** and **L2**, respectively.

Compounds	Metal (M)	Association constants (LogK$_{ass.}$), L:M	LOD (μM)	LOQ (μM)
L1	Cu^{2+}	5.11 ± 0.06 (1:1)	7.5	15.0
	Hg^{2+}	5.00 ± 0.01 (1:1)	8.0	14.0
L2	Cu^{2+}	4.59 ± 0.01 (1:1)	6.0	13.5
	Hg^{2+}	6.38 ± 0.06 (1:1)	2.5	4.50

The stability constants reveal the formation of mononuclear species for Cu^{2+} and Hg^{2+} in both compounds. The highest constant was obtained for compound **L2** for Hg^{2+} with a value of LogK$_{ass.}$ = 6.38 ± 0.06.

The lowest detectable and quantifiable amounts were also determined for **L2** (2.5 μM and 4.5 μM), indicating that it has a high affinity for binding with Hg^{2+} ions, having the potential to be useful in applications such as environmental monitoring, where the presence of Hg^{2+} needs to be detected and quantified at low concentrations.

The structure of **L2** seems to play a significant role in the observed values. The absence of benzene moiety in the dansyl-derived fluorophore reduces the stereochemical hindrance, making it easier and more accessible for the metal ion to coordinate with the ligand.

3.4.   Exploring dansyl derivatives behaviour in aqueous media

In order to understand the stability of the compounds in water, **L1** and **L2** were measured by absorption and emission in different mixtures, varying the ratio of acetonitrile to water. As can be seen in Figure 4 the increase of water led to a decrease in the emission intensity in both compounds up to 67% of water, after that value in 83% of water, an increased of the baseline was observed, which is indicative of the formation of aggregates. Moreover, an increase in the emission intensity and a blue shift are observed, surpassing in the case of **L1**, the emission intensity of the ligand in 100 % of acetonitrile.
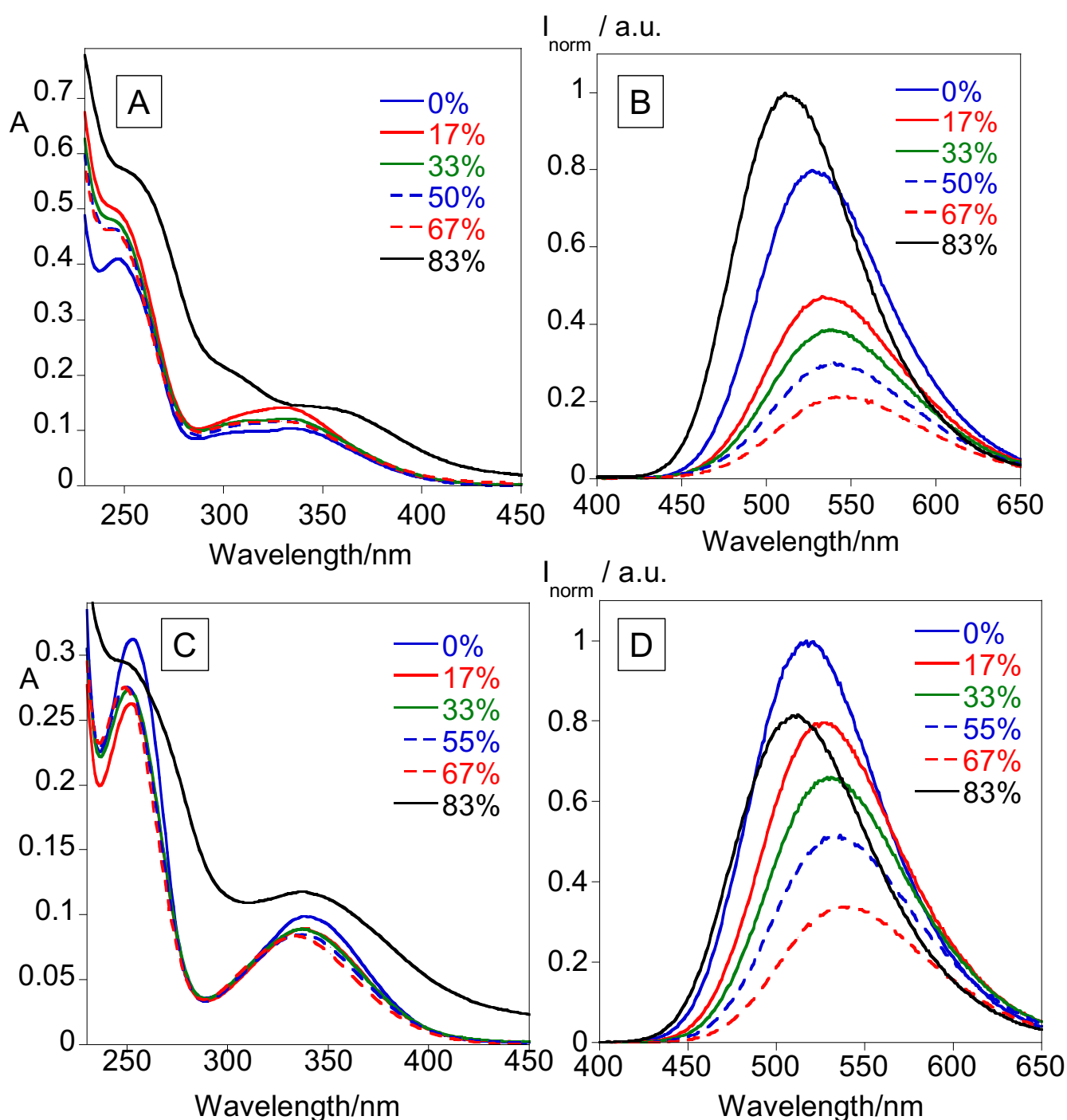
Figure 4. Absorption (A, C) and emission spectra (B, D) of **L1** (A,B) and **L2** (C,D) in CH$_3$CN with different water fraction f_w (0%, 17%, 33%, 55%, 67%, 83%). [**L1**]=[**L2**] = 10 μM, T = 298K.

Such behaviour was confirmed by the emission observed under the UV light lamp (see Figure 5), where the sample containing 83% of water appears to be the most emissive in both cases. The fluorescence quantum yield was determined, and a value of ϕ = 25% and ϕ = 13% were calculated for **L1** and **L2**, respectively. In the case of **L1** the fluorescence quantum yield was similar to the one observed in acetonitrile.

To explore deeply this observation, the solutions were measured by dynamic light scattering, resulting in monodispersed peaks (PDI $_{L1}$ = 0.02; PDI $_{L2}$ = 0.06) with hydrodynamic sizes of 124 ± 2 nm (**L1**) and 188 ±1.6 nm (**L2**).
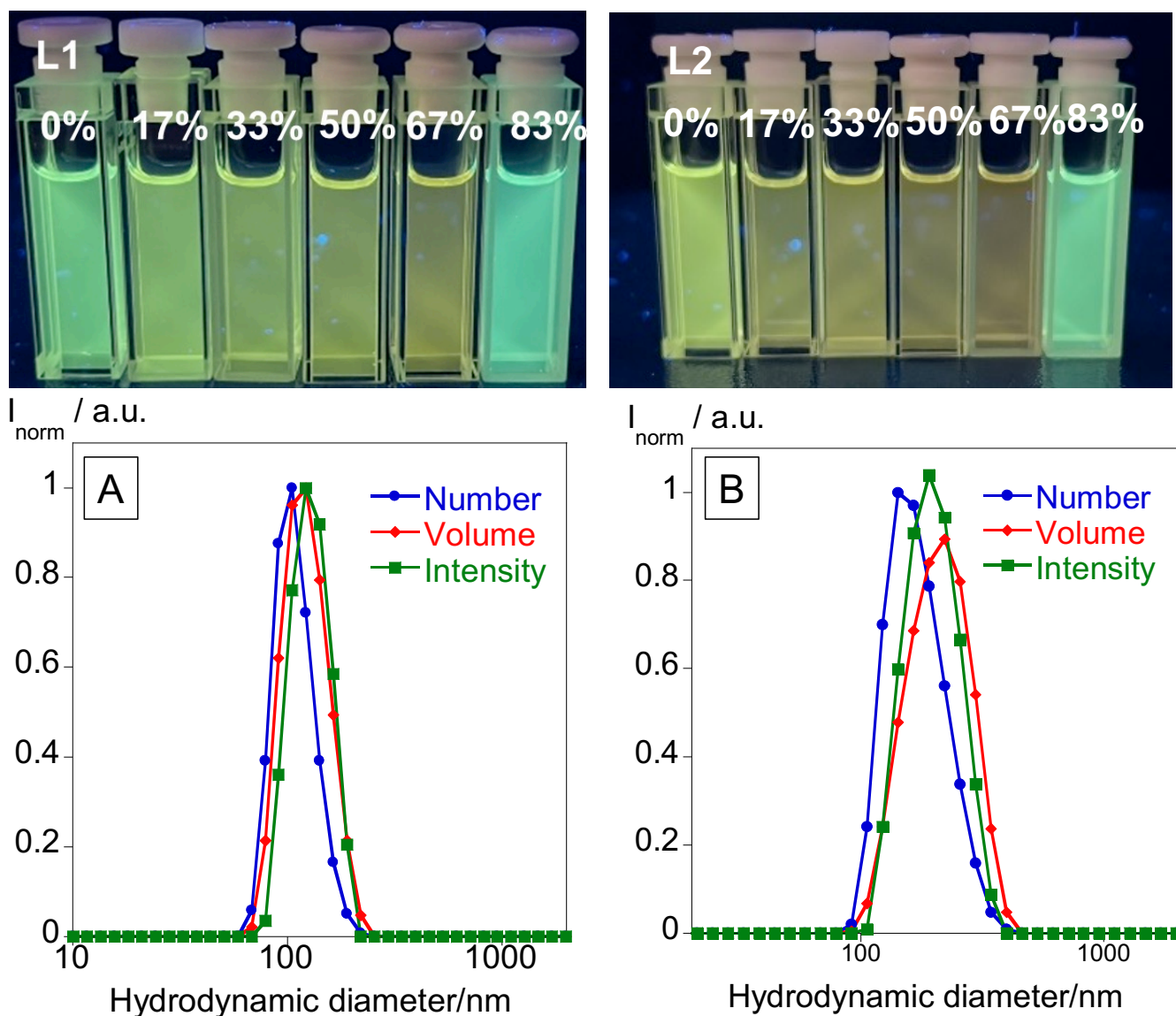
Figure 5. (Top) Images of **L1** and **L2** in CH_3CN with different water fraction f_w (0%, 17%, 33%, 55%, 67%, 83%). [**L1**]=[**L2**] = 10 µM, T = 298K. Size according to number, volume, and intensity distributions of a solution of CH_3CN/water solution of **L1** (A) and **L2** (B) with f_w = 83%.

These results confirmed the formation of aggregates in **L1** and **L2**. Based on other examples reported in the literature [18], herein the water modulates the aggregation state of the chromophore resulting in fluorescence enhancement *via* AIE mechanism, providing a wide range of multiple applications in complex environments. However, these organic compounds could present some drawbacks, such as poor water solubility, leading to latter precipitation of the aggregates.

3.5. L1 doped SBS polymeric nanoparticles

Due to the observed AIE phenomenon of current compounds in aqueous media and our past works concerning the development of systems that would allow highly hydrophobic and water quenched sensors to maintain their properties in water, Poly(styrene-butadiene-styrene) SBS polymeric

microparticles containing compound **L1** were synthesized using the precipitation method, a green method that minimizes waste generation [27], [28]. SBS matrix was chosen due to its intrinsic chemical formula, the presence of benzene moieties would potentially improve the stability of these microparticles by staking interactions with the same moiety present in the ligand.

The use of polymeric particles was in this case applied as a measure to enhance the dispersion of the ligand in aquous media, as well as for improving the AIE effect´s stability and bioavailability of the compound. The resulting SBS particles were characterized by fluorescence emission, dynamic light scattering (DLS) and transmission electron microscopy (TEM).

The dansyl-derivative **L1** is highly hydrophobic, but when incorporated into a polymeric matrix leads to stable and highly emissive microparticles soluble in water, with a fluorescence quantum yield of 22%.
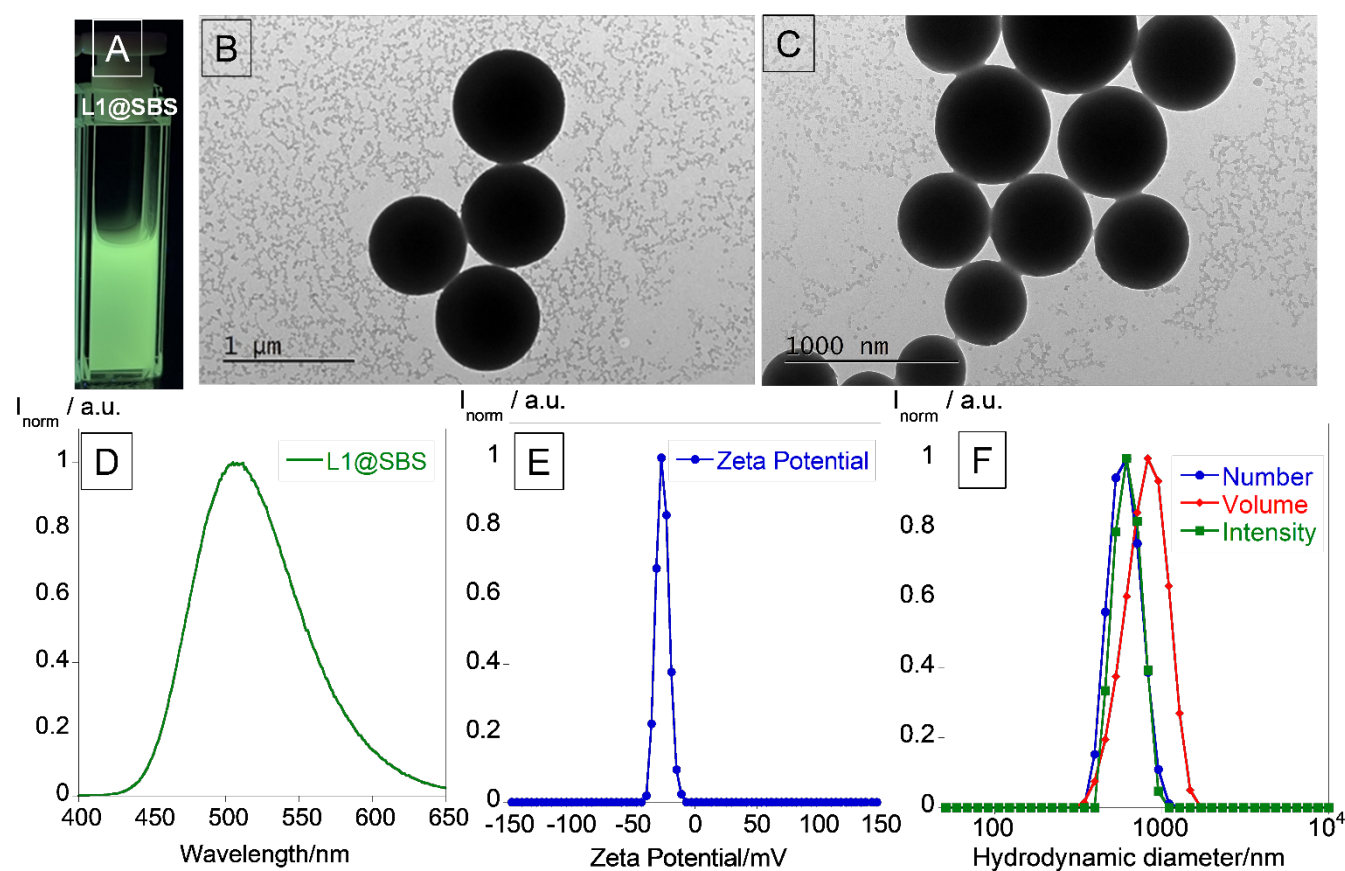
Figure 6. (A) Image of **L1**@SBS particles under UV-lamp; (B, C) TEM images of the **L1**@SBS particles, (D, E and F) Emission spectrum, zeta potential and hydrodynamic size of **L1**@SBS particles.

The results showed that the particles presented a spherical shape and that the ligand was successfully encapsulated within the polymeric matrix (see Figure 6), resulting in high emissive microparticles, with green emission and a maximum emission band at 505 nm in water. Additionally, the microparticles present a size of 628 ± 22 nm (PDI: 0.07±0.04) by DLS, a zeta potential of -27 ± 0.7, and a size of 520 ± 76 nm measured by TEM.

In this work, the use of SBS particles as a carrier for dansyl derivative **L1** has the potential to improve its solubility, stability, and bioavailability, making it a promising approach for drug delivery and other sensing applications.

4. Conclusions

In current work, we present the synthesis of two fluorescent sensors abbreviated as **L1** and **L2**, bearing dual dansyl moieties linked together by a disulfide bridge. Implementation of a classical condition of peptide synthesis for compound **L1** was used for the introduction of the benzene moiety, in order to tune the photophysical characteristics of this fluorophore in relation to **L2**. Due to the common knowledge of the dansyl derivatives to manifest solvatofluorochromism, extensive work has been carried out aiming to better understand the effect of different solvents on the emission properties. Positive solvatofluorochromism was observed for both **L1** and **L2** chromophores, and the Kamlet-Taft equation was applied to further understand the solute-solvent interactions. Alongside that, the presence of heteroatoms plays a crucial role in the sensing of metal ions, and so **L1** and **L2** were used as sensors to shed light on their potential for environmental remediation. Both compounds have been found to modulate their photophysical characteristics in the presence of Hg^{2+} and Cu^{2+} with quenching of the emission signal. Stability association constants and stoichiometry suggest mononuclear species for Cu^{2+} and Hg^{2+} in both compounds. Compound **L2** was found to exhibit the highest constant towards Hg^{2+} with a value of $LogK_{ass.} = 6.38$ with a LOD and LOQ of 2.5 μM and 4.5 μM. With the intention to further explore these compounds, their behavior in water was studied and found to manifest AIE enhancement at high fractions of water content with the formation of aggregates, as DLS suggests, with hydrodynamic sizes of 124 ± 2 nm (**L1**) and 188 ±1.6 nm (**L2**). Being in line with our previous efforts to characterize compounds once hydrophobic and unable to manifest emission properties due to water acting as a quencher, SBS polymeric doped microparticles were synthesized using an oil-in-water approach doped with **L1** to stabilize the AIE effect. TEM images suggest the formation of stable microparticles with a size of 520 ± 76 nm showing a green emission centred at 505 nm in water. Therefore, dansyl-derived compounds still provide value for their great photophysical characteristics, alongside their potential for metal ion sensing and as important molecules for bioimaging systems.

CRediT authorship contribution statement

Frederico Duarte: Formal analysis, Investigation, Writing - Original Draft, Writing - Review & Editing, Visualization.
Georgi Dobrikov: Methodology, Validation, Formal Analysis, Investigation, Writing - Original Draft, Writing - Review & Editing, Resources, Visualization.
Atanas Kurutos: Methodology, Validation, Formal Analysis, Investigation, Writing - Original Draft, Writing - Review & Editing, Resources, Visualization.

Javier Fernandez Lodeiro: Investigation, Resources, Validation, Writing - Review & Editing.

Jose Luis Capelo-Martinez: Resources, Writing - Review & Editing, Funding acquisition.

Hugo M. Santos: Investigation, Resources, Validation, Writing - Review & Editing.

Elisabete Oliveira: Conceptualization, Methodology, Validation, Formal Analysis, Investigation, Resources, Writing - Original Draft, Writing - Review & Editing, Resources, Visualization, supervision, Funding acquisition.

Carlos Lodeiro: Conceptualization, Methodology, Validation, Formal Analysis, Investigation, Resources, Writing - Review & Editing, Resources, Visualization, supervision, Funding acquisition, Project administration

Declaration of Competing Interest

The authors declare that they have no known competing financial interests or personal relationships that could have appeared to influence the work reported in this paper.

Data Availability

Data will be made available on request.

Acknowledgements

Appendix A. Supplementary material

References

[1] Zhang Y, Lei B, Zhang X. Intramolecular energy transfer dyes as temperature- and polarity-sensitive fluorescence probes. Dyes and Pigments 2022;205:110492. https://doi.org/10.1016/j.dyepig.2022.110492.

[2] Reisch A, Klymchenko AS. Fluorescent Polymer Nanoparticles Based on Dyes: Seeking Brighter Tools for Bioimaging. Small 2016;12:1968–92. https://doi.org/10.1002/smll.201503396.

[3] Nishiyabu R, Sugino Y, Kubo Y. White-light emitting boronate microparticles for potential use as reusable bright chemosensors in water. Chemical Communications 2013;49:9869. https://doi.org/10.1039/c3cc45739g.

[4] Cui Y, Li F, Zhang X. Controlling fluorescence resonance energy transfer of donor–acceptor dyes by Diels–Alder dynamic covalent bonds. Chemical Communications 2021;57:3275–8. https://doi.org/10.1039/D1CC00165E.

[5] Sierra AF, Hernández-Alonso D, Romero MA, González-Delgado JA, Pischel U, Ballester P. Optical Supramolecular Sensing of Creatinine. J Am Chem Soc 2020;142:4276–84. https://doi.org/10.1021/jacs.9b12071.

[6] Pan Y, Zhang C, Liu SH, Tan Y, Yin J. Fluorescent switch based on dithienylethene with dansulfonamide in multimedium. Dyes and Pigments 2020;181:108546. https://doi.org/10.1016/j.dyepig.2020.108546.

[7] Zhang Y, Lei B, Zhang X. Reversible, controllable white-light emission of dye systems by dynamic covalent furan moiety exchange. Chemical Communications 2022;58:5261–4. https://doi.org/10.1039/D2CC01309F.

[8] Shi Z, Wu J, Song Q, Göstl R, Herrmann A. Toward Drug Release Using Polymer Mechanochemical Disulfide Scission. J Am Chem Soc 2020;142:14725–32. https://doi.org/10.1021/jacs.0c07077.

[9] Dare EO, Vendrell-Criado V, Jiménez MC, Pérez-Ruiz R, Díaz Díaz D. Highly efficient latent fingerprint detection by eight-dansyl-functionalized octasilsesquioxane nanohybrids. Dyes and Pigments 2021;184:108841. https://doi.org/10.1016/j.dyepig.2020.108841.

[10] Pazin WM, Almeida AKA, Manzoni V, Dias JMM, de Abreu ACF, Navarro M, et al. Thermal and solvatochromic effects on the emission properties of a thienyl-based dansyl derivative. RSC Adv 2020;10:28484–91. https://doi.org/10.1039/D0RA05949H.

[11] Jiang H, Li Z, Kang Y, Ding L, Qiao S, Jia S, et al. A two-photon fluorescent probe for Cu2+ based on dansyl moiety and its application in bioimaging. Sens Actuators B Chem 2017;242:112–7. https://doi.org/10.1016/j.snb.2016.11.033.

[12] Thangaraj A, Bhardwaj V, Sahoo SK. A multi-analyte selective dansyl derivative for the fluorescence detection of Cu(II) and cysteine. Photochemical & Photobiological Sciences 2019;18:1533–9. https://doi.org/10.1039/c9pp00080a.

[13] Wang Y, Zhou J, Zhao L, Xu B. A dual-responsive and highly sensitive fluorescent probe for Cu^{2+} and pH based on a dansyl derivative. Dyes and Pigments 2020;180:108513. https://doi.org/10.1016/j.dyepig.2020.108513.

[14] Luo J, Xie Z, Lam JWY, Cheng L, Tang BZ, Chen H, et al. Aggregation-induced emission of 1-methyl-1,2,3,4,5-pentaphenylsilole. Chemical Communications 2001:1740–1. https://doi.org/10.1039/b105159h.

[15] Zhang J, Shen H, Liu X, Yang X, Broman SL, Wang H, et al. A Dihydroazulene-Based Photofluorochromic AIE System for Rewritable 4D Information Encryption. Angewandte Chemie International Edition 2022;61. https://doi.org/10.1002/anie.202208460.

[16] Ruan Y-B, Depauw A, Leray I. Aggregation-induced emission enhancement upon Al^{3+} complexation with a tetrasulfonated calix[4]bisazacrown fluorescent molecular sensor. Org Biomol Chem 2014;12:4335–41. https://doi.org/10.1039/C4OB00187G.

[17] Gao M, Tang BZ. Fluorescent Sensors Based on Aggregation-Induced Emission: Recent Advances and Perspectives. ACS Sens 2017;2:1382–99. https://doi.org/10.1021/acssensors.7b00551.

[18] Ruan Z, Zheng H, Deng C, Cheng X, Ruan X, Lv S, et al. A simple AIE-active triphenylamine derivative for supersensitive detection of water in organic solvents with noticeable fluorescence color change. Dyes and Pigments 2022;204:110476. https://doi.org/10.1016/j.dyepig.2022.110476.

[19] Sun H, Tang X-X, Miao B-X, Yang Y, Ni Z. A new AIE and TICT-active tetraphenylethene-based thiazole compound: Synthesis, structure, photophysical properties and application for water detection in organic solvents. Sens Actuators B Chem 2018;267:448–56. https://doi.org/10.1016/j.snb.2018.04.022.

[20] Song Z, Zhang W, Jiang M, Sung HHY, Kwok RTK, Nie H, et al. Synthesis of Imidazole-Based AIEgens with Wide Color Tunability and Exploration of their Biological Applications. Adv Funct Mater 2016;26:824–32. https://doi.org/10.1002/adfm.201503788.

[21] Wang J, Zhang X, Liu H-B. Highly sensitive pyrene–dansyl conjugate-based fluorescent sensor for discriminative detection of water in organic solvents. Dyes and Pigments 2020;182:108685. https://doi.org/10.1016/j.dyepig.2020.108685.

[22] Alam P, Leung NLC, Zhang J, Kwok RTK, Lam JWY, Tang BZ. AIE-based luminescence probes for metal ion detection. Coord Chem Rev 2021;429:213693. https://doi.org/10.1016/j.ccr.2020.213693.

[23] Wan H, Xu Q, Gu P, Li H, Chen D, Li N, et al. AIE-based fluorescent sensors for low concentration toxic ion detection in water. J Hazard Mater 2021;403:123656. https://doi.org/10.1016/j.jhazmat.2020.123656.

[24] Jiang Y, McNeill J. Light-Harvesting and Amplified Energy Transfer in Conjugated Polymer Nanoparticles. Chem Rev 2017;117:838–59. https://doi.org/10.1021/acs.chemrev.6b00419.

[25] Wan Q, Huang Q, Liu M, Xu D, Huang H, Zhang X, et al. Aggregation-induced emission active luminescent polymeric nanoparticles: Non-covalent fabrication methodologies and biomedical applications. Appl Mater Today 2017;9:145–60. https://doi.org/10.1016/j.apmt.2017.06.004.

[26] Suriya Prabha A, Dorothy R, Jancirani S, Rajendran S, Singh G, Senthil Kumaran S. Recent advances in the study of toxicity of polymer-based nanomaterials. Nanotoxicity, Elsevier; 2020, p. 143–65. https://doi.org/10.1016/B978-0-12-819943-5.00007-5.

[27] Duarte F, Cuerva C, Fernández-Lodeiro C, Fernández-Lodeiro J, Jiménez R, Cano M, et al. Polymer Micro and Nanoparticles Containing B(III) Compounds as Emissive Soft Materials for Cargo Encapsulation and Temperature-Dependent Applications. Nanomaterials 2021;11:3437. https://doi.org/10.3390/nano11123437.

[28] González-Tobío B, Duarte F, Arribas-Delgado A, Fernández-Lodeiro C, Fernández-Lodeiro J, Cano M, et al. Tuning and reviving the luminescence of a new class of pyridyl β-

diketonate Eu(III) metallomesogens: From molecules to entrapment in polymer particles. Dyes and Pigments 2022;204:110440. https://doi.org/10.1016/j.dyepig.2022.110440.

[29] Zhang X, Wang K, Liu M, Zhang X, Tao L, Chen Y, et al. Polymeric AIE-based nanoprobes for biomedical applications: recent advances and perspectives. Nanoscale 2015;7:11486–508. https://doi.org/10.1039/C5NR01444A.

[30] Lodeiro C, Capelo JL, Mejuto JC, Oliveira E, Santos HM, Pedras B, et al. Light and colour as analytical detection tools: A journey into the periodic table using polyamines to bio-inspired systems as chemosensors. Chem Soc Rev 2010;39:2948. https://doi.org/10.1039/b819787n.

[31] Lodeiro C, Lima JC, Parola AJ, Seixas de Melo JS, Capelo JL, Covelo B, et al. Intramolecular excimer formation and sensing behavior of new fluorimetric probes and their interactions with metal cations and barbituric acids. Sens Actuators B Chem 2006;115:276–86. https://doi.org/10.1016/j.snb.2005.09.010.

[32] Lodeiro C, Pina F. Luminescent and chromogenic molecular probes based on polyamines and related compounds. Coord Chem Rev 2009;253:1353–83. https://doi.org/10.1016/j.ccr.2008.09.008.

[33] Moura NMM, Núñez C, Santos SM, Faustino MAF, Cavaleiro JAS, Neves MGPMS, et al. Synthesis, Spectroscopy Studies, and Theoretical Calculations of New Fluorescent Probes Based on Pyrazole Containing Porphyrins for Zn(II), Cd(II), and Hg(II) Optical Detection. Inorg Chem 2014;53:6149–58. https://doi.org/10.1021/ic500634y.

[34] Lamelas R, García V, Liñares A, Bastida R, Labisbal E, Fernández-Lodeiro A, et al. Novel trans-disubstituted hexaaza-macrocyclic ligands containing pyridine head units: Synthesis, disubstitution and colorimetric properties. Sens Actuators B Chem 2016;225:481–91. https://doi.org/10.1016/j.snb.2015.11.090.

[35] Gonc AC, Luis J, Lodeiro C, Dos AA. Sensors and Actuators B : Chemical A seleno-pyrene selective probe for Hg^{2+} detection in either aqueous or aprotic systems 2017;239:311–8. https://doi.org/10.1016/j.snb.2016.08.014.

[36] Oliveira E, Núñez C, Santos HM, Fernández-Lodeiro J, Fernández-Lodeiro A, Capelo JL, et al. Revisiting the use of gold and silver functionalised nanoparticles as colorimetric and fluorometric chemosensors for metal ions. Sens Actuators B Chem 2015;212:297–328. https://doi.org/10.1016/j.snb.2015.02.026.

[37] Pedro G, Duarte F, Cheptsov DA, Volodin NYu, Ivanov I V., Santos HM, et al. Exploring Coumarin-Based Boron Emissive Complexes as Temperature Thermometers in Polymer-Supported Materials. Sensors 2023;23:1689. https://doi.org/10.3390/s23031689.

[38] M. Montalti, A. Credi, L. Prodi MG, Montalti M, Credi A, Prodi L GM. Handbook of Photochemistry. 3rd ed. BOCA: Taylor & Francis, Boca Raton; 2006.

[39] Youziel J, Akhbar AR, Aziz Q, Smith MEB, Caddick S, Tinker A, et al. Bromo- and thiomaleimides as a new class of thiol-mediated fluorescence 'turn-on' reagents. Org Biomol Chem 2014;12:557–60. https://doi.org/10.1039/C3OB42141D.

[40] Espinar-Barranco L, Luque-Navarro P, Strnad MA, Herrero-Foncubierta P, Crovetto L, Miguel D, et al. A solvatofluorochromic silicon-substituted xanthene dye useful in bioimaging. Dyes and Pigments 2019;168:264–72. https://doi.org/10.1016/j.dyepig.2019.04.024.

[41] Ghanadzadeh Gilani A, Moghadam M, Zakerhamidi MS. Solvatochromism of Nile red in anisotropic media. Dyes and Pigments 2012;92:1052–7. https://doi.org/10.1016/j.dyepig.2011.07.018.

[42] Nootem J, Sattayanon C, Namuangruk S, Rashatasakhon P, Wattanathana W, Tumcharern G, et al. Solvatochromic triazaborolopyridinium probes toward ultra-sensitive trace water detection in organic solvents. Dyes and Pigments 2020;181:108554. https://doi.org/10.1016/j.dyepig.2020.108554.

[43] GANS P, SABATINI A, VACCA A. Investigation of equilibria in solution. Determination of equilibrium constants with the HYPERQUAD suite of programs. Talanta 1996;43:1739–53. https://doi.org/10.1016/0039-9140(96)01958-3.